Development of a MEMS-Scale Photoacoustic Chemical Sensor Using a Quantum Cascade Laser

Ellen L. Holthoff, David A. Heaps, and Paul M. Pellegrino

Invited Paper

Abstract—The development of a microelectromechanical systems-scale photoacoustic chemical sensor is described. Specifically, both a pulsed and a modulated continuous wave quantum cascade laser were used to determine detection limits for dimethyl methylphosphonate (DMMP), a standard nerve gas simulant. These sources were continuously tunable from 9.3 to 10 μm. We report a minimum detection level of 20 parts-per-billion (ppb) and exceptional agreement between the measured photoacoustic vibrational spectrum and the IR spectrum of DMMP. The results support the continued development of a miniaturized photoacoustic sensor.

Index Terms—Microelectromechanical system (MEMS), photoacoustic spectroscopy (PAS), quantum cascade laser (QCL), sensor.

I. INTRODUCTION

THE global war on terror has made rapid detection and identification of chemical and biological agents a priority for military and homeland defense applications. Reliable real-time detection of these threats is complicated by our enemy's use of a diverse range of materials, including chemical and biological warfare agents and toxic industrial chemicals. Therefore, an adaptable sensor platform is necessary for detecting and identifying the threat agents before they cause harm. The 1995 deployments of sarin nerve gas in the Tokyo subway system by members of the Aum Shinrikyo cult [1], the 2001 anthrax attacks in the United States [2], the false-alarm evacuation of the Russell Senate Office Building in February of 2006 [3], and the recent use of chlorine gas in Iraq [4] are just a few examples demonstrating the need for extremely sensitive and selective sensor systems.

Photothermal spectroscopy (PAS) encompasses a group of highly sensitive methods that can be used to detect trace levels of gases using optical absorption and subsequent thermal perturbations of the gases. The underlying principle that connects these various spectroscopic methods is the measurement of physical changes (i.e., temperature, density, or pressure) as a result of photoinduced change in the thermal state of the sample. In general, photothermal methods are classified as indirect methods for detection of trace optical absorbance, because the transmission of the light used to excite the sample is not measured directly. Examples of photothermal techniques include photothermal interferometry, photothermal lensing, photothermal deflection, and PAS. In comparison to other photothermal techniques, which measure the refractive index using combinations of probe sources and detectors, PAS measures the pressure wave produced by sample heating. Recent research suggests that PAS is a particularly sensitive technique, capable of trace gas detection at parts-per-trillion (ppt) levels [5], [6]. Although these studies demonstrate the sensitivity capabilities of photoacoustic sensors, the total system size represents a large logistics burden in terms of size, cost, and power consumption.

To date, limited research has been done to demonstrate the feasibility of a miniaturized photoacoustic sensor [7]–[13]. Initial examination of the scaling principles associated with PAS in respect to microelectromechanical systems (MEMS) dimensions indicated that photoacoustic signals would remain at similar sensitivities or even surpass those commonly found in macroscale devices [7]–[12]. Recently, we demonstrated the use of a CO_2 laser-based MEMS-scale photoacoustic sensor to provide detection limits at parts-per-billion (ppb) levels for the nerve gas simulant, dimethyl methylphosphonate (DMMP) [12]. However, CO_2 lasers are relatively bulky and consume large amounts of power. In order to realize the advantage of photoacoustic sensor miniaturization, light sources of comparable size are required. In present study, we report on the use of a continuously tunable quantum cascade laser (QCL), in combination with a MEMS-scale photoacoustic cell design, for detection of DMMP.

II. BACKGROUND

In order to generate acoustic waves in gases, periodic heating and cooling of the sample is required to produce pressure fluctuations. This is accomplished using modulated or pulsed excitation sources [14]–[16]. The pressure waves detected in PAS are generated directly by the absorbed fraction of the modulated or pulsed excitation beam. Therefore, the signal generated from a photoacoustic experiment is directly proportional to the absorbed incident power.

E. L. Holthoff and P. M. Pellegrino are with the U.S. Army Research Laboratory, Adelphi, MD 20783 USA (e-mail: ellen.holthoff@us.army.mil; ppellegr@arl.army.mil).

D. A. Heaps is with Astra Zeneca Pharmaceuticals LP, Wilmington, DE 19850 USA (e-mail: david.heaps@astrazeneca.com).

A. Modulated Excitation

In the case of optically chopped continuous wave (CW) lasers or modulated sources, the relationship between the generated signal and the absorbed power at a given wavelength (λ) can be written as [17]–[19]

$$S = CP_0(\lambda)\alpha(\lambda). \tag{1}$$

In this expression, S denotes the photoacoustic signal, C is a cell-specific constant, P_0 signifies the incident power, and α is the sample absorption coefficient, where $\alpha = N\sigma$ and N is the gas concentration and σ denotes the absorption cross section.

C is a function of cell geometry, measurement conditions, and modulation frequency. If the modulation frequency differs from an acoustic resonance frequency of the photoacoustic cell, the system is operating in a nonresonant mode, and C is described by [18], [20], [21]

$$C = \frac{(\gamma - 1)l}{i\omega V}. \tag{2}$$

Here, γ denotes the adiabatic coefficient of the gas, l represents the resonator length, i is an imaginary unit, ω represents the angular frequency of modulation, and V is the volume of the cell.

When the modulation frequency is the same as an acoustic resonance frequency of the photoacoustic cell, the resonant eigenmodes of the cell can be excited, resulting in an amplification of the signal [22]–[25] by a quality factor Q [26], where

$$Q = \frac{f_0}{\Delta f}. \tag{3}$$

In this expression, Δf denotes the full-width at half-maximum (FWHM) of the resonance profile and f_0 is the resonance frequency of the cell, which is described by [6] and [27]

$$f_0 = \frac{c}{2l}. \tag{4}$$

Here, c is the speed of sound at a given temperature. The behavior of Q can be derived from cell geometry. For a cell of radius r and length $l \gg r$ operated at a longitudinal mode

$$Q \propto \frac{r}{\sqrt{l}}. \tag{5}$$

The proportionality (5) indicates a reduction in Q as the cell is scaled downward [27]. In the resonant case, C is described by [18], [21], and [28]

$$C = Q_j \frac{(\gamma - 1)F_j}{\omega_j V} \tag{6}$$

where Q_j and ω_j belong to the jth eigenmode, and F_j is a factor that depends on the positions of the source and microphone, relative to the jth eigenmode distribution.

B. Pulsed Excitation

In the case of pulsed sources, each pulse generates an exponentially decaying sine wave with an amplitude described by [28]

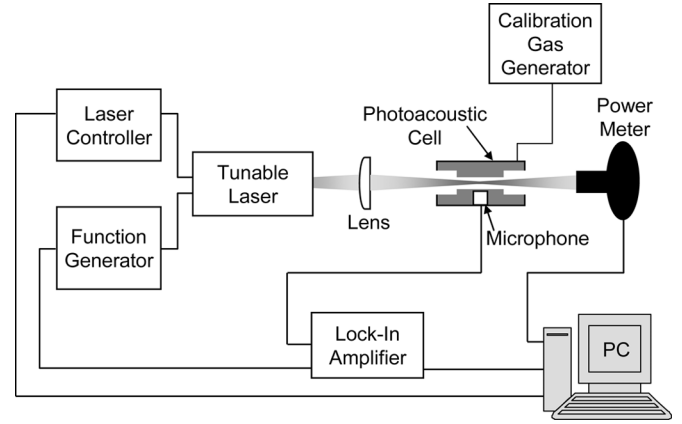$$S = \frac{F(\gamma - 1)}{V} E\alpha \tag{7}$$

Fig. 1. Simplified diagram of a typical photoacoustic gas sensor system. Electronic connections are indicated by a solid line.

where E is the pulse energy. In this case, C is strictly dependent on the geometrical properties of the photoacoustic cell.

III. PHOTOACOUSTIC SENSOR SYSTEM PLATFORM

Fig. 1 depicts a block diagram of the basic elements required for a photoacoustic gas sensor.

A. Quantum Cascade Laser

A broadly tunable, external cavity QCL (Daylight Solutions, Inc.) was employed as the excitation source for the sensing system. The laser was powered by an external controller (Daylight Solutions, Inc., model: TLC 1001). Both a pulsed (model: 10080) and a modulated CW (model: 21096) source were investigated. Both lasers operated at a center wavelength of 9.6 μm, with a scanning range up to 100 cm^{-1} and spectral resolution better than 1 cm^{-1}. The transmitted laser power was measured with a power meter (Ophir Optronics, model: Nova II) equipped with a thermal head (Ophir Optronics, model: 3A). These measurements allowed for normalization of the photoacoustic signal for any residual drift associated with the excitation source.

1) Pulsed QCL: The pulsed source operated at room temperature with convective cooling. Current pulses of 1650 mA with a 500 ns duration and 20.9 kHz pulse rate corresponded to a 1.0% duty cycle and provided an average optical power of 1.35 (±0.02) mW. A KBr planoconvex lens (ISP Optics, model: custom) was utilized for focusing purposes.

2) Modulated CW QCL: The modulated CW source required a compact chiller (Solid State Cooling Systems, model: Oasis 150). An injection current of 725 mA provided an average optical power of 11.97 (±0.03) mW. A function generator (Stanford Research Systems, model: DS340) was connected to the laser head via a subminiature version A connector to allow for external current modulation. A 17.2 kHz sine wave with a peak amplitude of 2.5 V resulted in 65% amplitude modulation. Beam focusing was accomplished using a CaF$_2$ planoconvex lens (ISP Optics, model: custom).

B. MEMS-Scale Photoacoustic Cell

A MEMS-scale differential photoacoustic cell was fabricated to meet our design specifications [29] by Infotonics Tech-
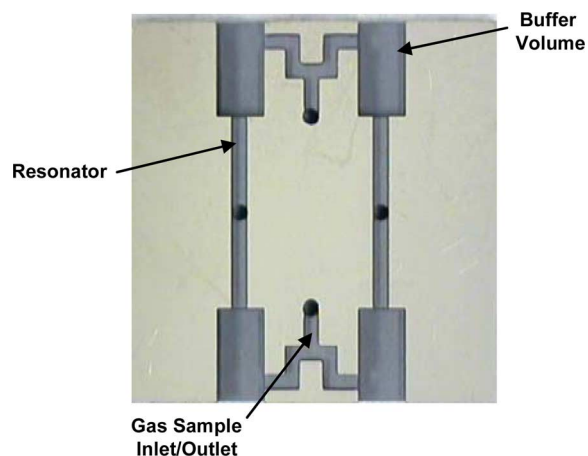
Fig. 2. Photograph of the internal structure of the MEMS-scale photoacoustic cell.

Fig. 3. Photograph of the fabricated MEMS-scale photoacoustic cell used when collecting data.

nology Center, Inc. The differential technique employs two resonator tubes, both housing a microphone (Knowles, model: FG-23629), but with radiation directed only through one to generate a photoacoustic signal. The microphones possessed similar responsivities, which allowed for subtraction of the reference microphone signal from the photoacoustic microphone signal. This allowed for the removal of noise elements that were present in both resonant chambers, such as external vibrations.

The influence of cell geometry on the photoacoustic signal has been discussed elsewhere [6]. Briefly, the cell consisted of two 10-mm-long open resonators having square cross sections, each with a diameter of 0.864 mm. The resonator was flanked on both sides by a buffer volume (acoustic filter), which provided noise suppression. The resonator length was twice that of the buffer volume, and the diameter of the buffer volume was at least three times that of the resonator. To further suppress gas flow noise, the cell had a convoluted, split sample inlet/outlet design (see Fig. 2).

The cell had two germanium windows (Edmund Optics, model: NT47-685), which were attached to the buffer volumes on either side of the photoacoustic resonator with epoxy. Small aluminum squares were attached to the buffer volumes on either side of the reference resonator with epoxy. Tygon tubing was connected to the buffer volumes to allow for gas sample inlet and outlet flow. The MEMS-scale photoacoustic cell was mounted between two printed circuit boards, which allowed for wiring the microphones to a power supply (AA battery) and a lock-in amplifier (via modified BNC cables). Fig. 3 is a photograph of the fabricated MEMS-scale photoacoustic cell.

C. Sample Generation

The trace gas (DMMP) was generated using a calibration gas generator (VICI Metronics, model: Dynacalibrator 190). The DMMP source was a certified permeation tube (VICI Metronics, model: Dynacal 107-150-7845-C100, length: 15 cm) that was placed in the generator oven held at a constant temperature of 100 °C. The permeation rate at this temperature was 1180 ng/min ($\pm 2\%$) and concentrations in the range of 1 part-per-million (ppm) to 380 ppb were produced by varying calibrated flows from 200 to 600 mL/min, respectively. Higher flow rates were avoided due to the onset of turbulent flow,
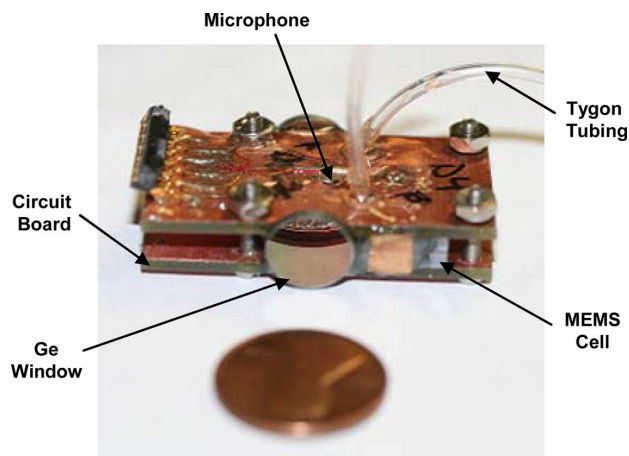
which dramatically increased the noise floor of the microphone. Nitrogen was used as the carrier gas. Polytetrafluoroethylene tubing was used to connect the gas generator to the sample inlet of the photoacoustic cell.

D. Data Acquisition

The signals detected by both the photoacoustic and the reference microphones were extracted using the differential voltage input on a lock-in amplifier (Stanford Research Systems, model: SR530) with a time constant of 3 s operating at the modulation or pulse frequency of the laser. LabVIEW (National Instruments, version 8.2) was used to create virtual instruments (VIs) to read and record the voltage outputs from the lock-in amplifier under various conditions directly to a PC. To estimate the limit of detection (LOD) of DMMP, the laser modulation, or pulse frequency and wavelength were held constant and the gas generator flow rate was ramped, which produced decreasing sample concentrations. The VI was programmed to collect the X (in-phase), Y (quadrature), R (amplitude), and θ (phase angle) components of the photoacoustic signal. The Y component was used for LOD determinations. Mean values and standard deviations of 200 points at a given concentration were calculated. The background signal, attributed to the absorbance of laser radiation by the cell windows and walls, was also measured. This background signal was subtracted from the mean photoacoustic signal measured at each concentration of DMMP. These values were used to prepare a linear regression with which the LOD could be calculated by taking three times the standard deviation (3σ) of the background and dividing it by the slope of the linear function.

IV. EXPERIMENTAL RESULTS AND DISCUSSION

The laser photoacoustic spectrum and limit of detection of DMMP were determined for the MEMS-scale photoacoustic sensor platform employing both a pulsed and modulated CW laser.

A. Pulsed QCL

The fundamental resonance mode of the MEMS-scale photoacoustic cell corresponding to (4) is approximately 17.2 kHz.
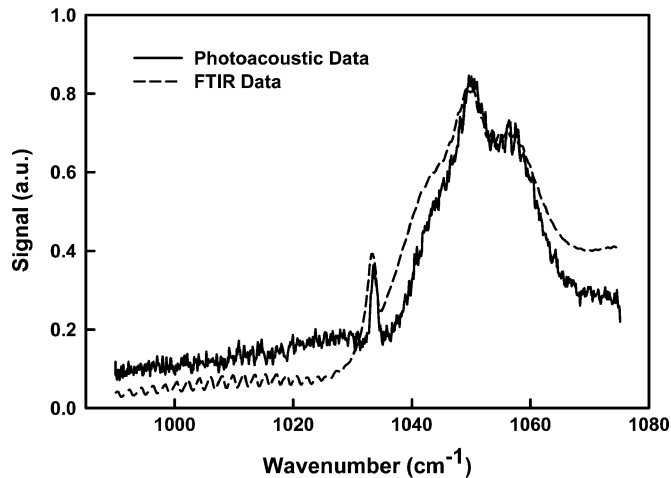
Fig. 4. Measured pulsed laser photoacoustic spectrum of 1.05 ppm DMMP in nitrogen gas compared to FTIR reference spectrum of DMMP.

Fig. 6. Measured modulated CW laser photoacoustic spectrum of 1.05 ppm DMMP in nitrogen gas compared to FTIR spectrum of DMMP.

B. Modulated CW QCL

The laser was externally modulated at 17.2 kHz, which is the fundamental resonance mode of the MEMS-scale photoacoustic cell corresponding to (4). The value of Q corresponding to (3) was approximately 5, which correlates well with the expected Q value for a cell of these dimensions.

The laser photoacoustic spectrum of DMMP was collected by scanning the wavelength range (9.34–9.95 μm) of the laser. Due to the mode hopping [31] nature of this source, continuous wavelength tunability over the entire tuning range required simultaneous control of the laser current and wavelength. While necessary for source stabilization, this process resulted in longer data acquisition times. However, high resolution may not be necessary to accurately record spectral detail of analytes having broad absorption features, such as DMMP. Therefore, a reduction in the number of measured wavelengths will maintain the structure of the DMMP absorption spectrum and decrease measurement times. We chose to investigate 102 wavelengths in the range of 9.34–9.69 μm (1070.0–1032.0 cm^{-1}). An important feature of this range is that the measurements were performed without any change in the laser current. Although mode hopping still occurs in this wavelength region, there is agreement between the laser photoacoustic data and the FTIR spectroscopy absorbance spectrum (see Fig. 6). Based on these data, the maximum DMMP absorbance in this region occurs at 9.50 μm (1053 cm^{-1}).

Fig. 7 illustrates the sensor response as a function of DMMP concentration measured at 9.50 μm. The 3σ limit of detection was determined to be 20 ppb for DMMP. The results exhibit excellent linearity with a correlation coefficient (R^2) of 0.9996.

The average optical power of the modulated CW QCL was significantly greater than the pulsed model. Therefore, based on (1), it was expected that the photoacoustic sensor system employing the modulated source would produce improved DMMP detection limits compared to the pulsed laser. Although this was the case, the limit of detection achieved using the pulsed QCL was better than initially anticipated, considering the nonresonant mode operation. This deviation may be an indication that the fundamental resonance mode of the MEMS-scale photoacoustic cell corresponding to (4) is not optimal for this structure.
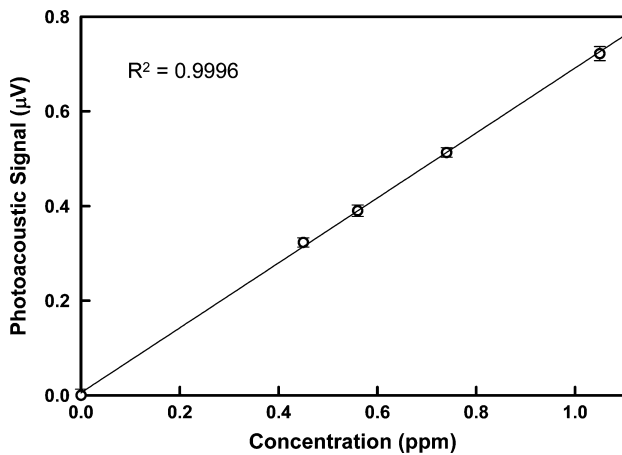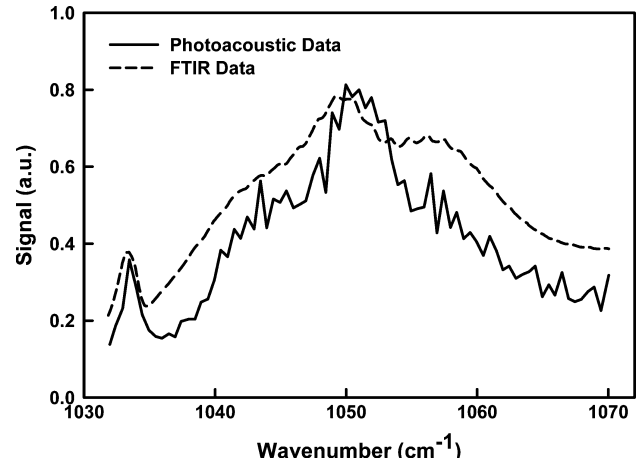

Fig. 5. Photoacoustic data attained using pulsed QCL as a function of DMMP concentration. Error bars represent one standard deviation and are barely visible. A linear function has been fit to the data. The 3σ LOD is 54 ppb.

Experimental characterization of the photoacoustic response of the sensor system demonstrated an optimized response at a slightly shifted frequency of 20.9 kHz. Several factors in the photoacoustic system, including increased microphone response; an increase in laser power due to pulse width limitations; and non-ideal resonance conditions may have contributed to the observed variance from the theoretical resonance mode.

The laser photoacoustic spectrum of DMMP was collected by scanning the wavelength range (9.30–10.10 μm or 1075.15–990.0 cm^{-1}) of the laser. This analyte has known absorption features in this region, assigned to phosphorusoxygencarbon stretching vibrations [30]. There is very good agreement between the laser photoacoustic data and the Fourier transform IR (FTIR) spectroscopy absorbance spectrum (see Fig. 4). Based on these data, the maximum DMMP absorbance in this region occurs at 9.50 μm (1053 cm^{-1}).

Fig. 5 illustrates the sensor response as a function of DMMP concentration measured at 9.50 μm. The 3σ limit of detection was determined to be 54 ppb for DMMP. The results exhibit excellent linearity with a correlation coefficient (R^2) of 0.9996.
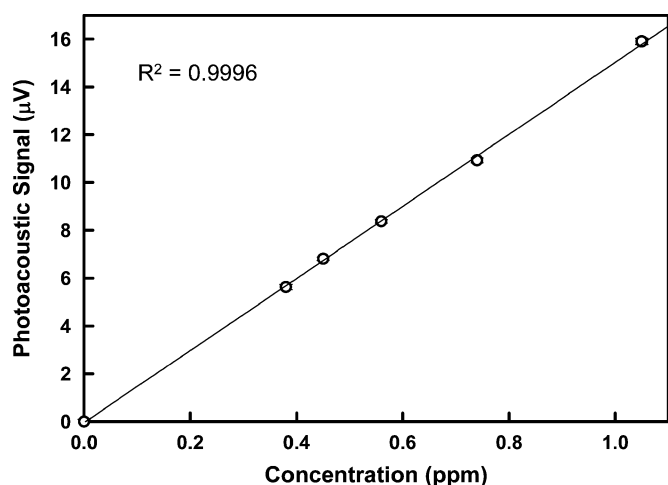
Fig. 7.   Photoacoustic data acquired using modulated CW QCL as a function of DMMP concentration. Error bars represent one standard deviation and are barely visible. A linear function has been fit to the data. The 3σ LOD is 20 ppb.

This could be a result of cell miniaturization as it relates to the acoustic theory that determines this resonance. Full modeling of the acoustic cavity, which takes into account the effects of the buffer volumes and convoluted sample inlet, is needed to resolve the optimal acoustic resonance frequency of the cell. This frequency can then be verified experimentally. Investigation of microphone frequency response, particularly at higher frequencies (20 to 30 kHz), is also needed. Finally, at these cell dimensions, the microphone may play a more significant role in the acoustical response of this system, rather than a passive monitor of the pressure wave produced in the photoacoustic cell. Therefore, it may be necessary to consider the microphone placement and acoustical character within the acoustic resonator in order to maximize the microphone response at the desired modulation frequency and ensure the optimal performance of this photoacoustic sensor.

Although the increased output power of the modulated CW laser afforded a better DMMP detection limit compared to that obtained using the pulsed source, consideration of power consumption and heat management may favor the use of a pulsed QCL for future sensor development. A pulsed QCL with increased optical output power and a repetition rate of the appropriate frequency may result in detection limits comparable to those realized with the modulated CW QCL.

As a final measure of the effectiveness of this sensing platform, we considered the recommended airborne exposure limits for a number of nerve agents [32]. For a 30 min exposure to relevant compounds, the lethal concentration is approximately 575 ppb, with the first noticeable heath effects occurring at 5.8 ppb. While we have not achieved the necessary detection limits in this report, we are confident that optimization of this MEMS-scale sensor will yield the desired results necessary to enable a compact sensor based on photoacoustic technology.

V. CONCLUSION

We have successfully demonstrated a MEMS-scale photoacoustic sensing platform, using continuously tunable pulsed and modulated CW QCL sources. These systems yield ppb detection

limits for DMMP. We are currently working toward sensor optimization, including the design and fabrication of new MEMS-scale photoacoustic cells with more efficient acoustic filters; investigating the acoustic theory that determines cell resonance frequency and how this relates to cell miniaturization; and improving the beam focus through the resonant cavity of the photoacoustic cell to reduce wall absorption. The latter is achieved by employing the appropriate optics to attain a decreased beam radius. This will result in little or no optical vignetting; thus increasing the amount of power available for molecular absorption and improving detection limits.

We believe that this sensor platform is an important step toward the development of a manportable prototype. In the future, combining multiple continuously tunable QCLs having different center wavelengths with a MEMS-scale photoacoustic cell would provide a broad wavelength tuning range, allowing for increased molecular discrimination and simultaneous detection of several molecules of interest.

REFERENCES

[1] A. T. Tu, "Overview of sarin terrorist attacks in Japan," *ACS Syp. Series*, vol. 745, pp. 304–317, 2000.
[2] D. Canedy and A. Kuczynski, *A Nation Challenged: A Medical Mystery*.   New York: The New York Times, Oct. 9, 2001.
[3] C. Williams, A. Lengel, and M. B. Sheridan, *Alarm Prompts Evacuation of Senate Offices*.   Washington, DC: The Washington Post, Feb. 9, 2006.
[4] K. Semple, *Suicide Bombers Using Chlorine Gas Kill 2 and Sicken Hundreds in Western Iraq*.   New York: The New York Times, Mar. 18, 2007.
[5] M. Nagele and M. W. Sigrist, "Mobile laser spectrometer with novel resonant multipass photoacoustic cell for trace-gas sensing," *Appl. Phys. B*, vol. 70, pp. 895–901, 2001.
[6] F. G. C. Bijnen, J. Reuss, and F. J. M. Harren, "Geometrical optimization of a longitudinal photoacoustic cell for a sensitive and fast trace gas detection," *Rev. Sci. Instrum.*, vol. 67, pp. 2914–2933, 1996.
[7] S. L. Firebaugh, K. F. Jensen, and M. A. Schmidt, "Miniaturization and integration of photoacoustic detection with a microfabricated chemical reactor system," *JMEMS*, vol. 10, pp. 232–237, 2001.
[8] S. L. Firebaugh, K. F. Jensen, and M. A. Schmidt, "Miniaturization and integration of photoacoustic detection," *J. Appl. Phys.*, vol. 92, pp. 1555–1563, 2002.
[9] P. Pellegrino and R. Polcawich, "Advancement of a MEMS photoacoustic chemical sensor," *Proc. SPIE*, vol. 5085, pp. 52–63, 2003.
[10] P. Pellegrino, R. Polcawich, and S. L. Firebaugh, "Miniature photoacoustic chemical sensor using microelectromechanical structures," *Proc. SPIE*, vol. 5416, pp. 42–53, 2004.
[11] D. A. Heaps and P. Pellegrino, "Examination of a quantum cascade laser source for a MEMS-scale photoacoustic chemical sensor," *Proc. SPIE*, vol. 6218, pp. 621805-1–621805-9, 2006.
[12] D. A. Heaps and P. Pellegrino, "Investigations of intraband quantum cascade laser source for a MEMS-scale photoacoustic sensor," *Proc. SPIE*, vol. 6554, pp. 65540F-1–65540F-9, 2007.
[13] U. Bonne, B. E. Cole, and R. E. Higashi, "Micromachined integrated opto-flow gas/liquid sensor," U.S. Patent 5 886 249, Mar. 23, 1999.
[14] C. K. N. Patel and A. C. Tam, "Pulsed optoacoustic spectroscopy of condensed matter," *Rev. Mod. Phys.*, vol. 53, pp. 517–550, 1981.
[15] J. B. Kinney and R. H. Staley, "Applications of photoacoustic spectroscopy," *Ann. Rev. Mater. Sci.*, vol. 12, pp. 295–321, 1982.
[16] A. C. Tam, "Applications of photoacoustic sensing techniques," *Rev. Mod. Phys.*, vol. 58, pp. 381–431, 1986.
[17] M. W. Sigrist, "Trace gas monitoring by laser photoacoustic spectroscopy and related techniques (plenary)," *Rev. Sci. Instrum.*, vol. 74, pp. 486–490, 2003.
[18] T. Schmid, "Photoacoustic spectroscopy for process analysis," *Anal. Bioanal. Chem.*, vol. 384, pp. 1071–1086, 2006.

[19] A. Elia, C. Di Franco, P. M. Lugarà, and G. Scamarcio, "Photoacoustic spectroscopy with quantum cascade lasers for trace gas detection," *Sensors*, vol. 6, pp. 1411–1419, 2006.

[20] F. J. M. Harren, G. Cotti, J. Oomens, and S. Te Lintel Hekkert, "Photoacoustic spectroscopy in trace gas monitoring," in *Encyclopedia of Analytical Chemistry*, R. A. Meyers, Ed. Chichester, U.K.: Wiley, 2000, pp. 2203–2226.

[21] M. W. Sigrist, "Air Monitoring by Laser Photoacoustic Spectroscopy," in *Air Monitoring by Spectroscopic Techniques*, M. W. Sigrist, Ed. New York: Wiley, 1994, pp. 163–238.

[22] C. F. Dewey, R. D. Kamm, and C. E. Hackett, "Acoustic amplifier for detection of atmospheric pollutants," *Appl. Phys. Lett.*, vol. 23, pp. 633–635, 1973.

[23] R. D. Kamm, "Detection of weakly absorbing gases using a resonant optoacoustic method," *J. Appl. Phys.*, vol. 47, pp. 3550–3558, 1976.

[24] A. Karbach and P. Hess, "High precision acoustic spectroscopy by laser excitation of resonator modes," *J. Chem. Phys.*, vol. 83, pp. 1075–1084, 1985.

[25] A. Miklós, P. Hess, and Z. Bozoki, "Application of acoustic resonators in photoacoustic trace gas analysis and metrology," *Rev. Sci. Instrum.*, vol. 72, pp. 1937–1955, 2001.

[26] R. E. Lindley, A. M. Parkes, K. A. Keen, E. D. McNaghten, and A. J. Orr-Ewing, "A sensitivity comparison of three photoacoustic cells containing a single microphone, a differential dual microphone, or a cantilever pressure sensor," *Appl. Phys. B*, vol. 86, pp. 707–713, 2007.

[27] S. Bernegger and M. W. Sigrist, "Longitudinal resonant spectrophone for CO-laser photoacoustic spectroscopy," *Appl. Phys. B*, vol. 44, pp. 125–132, 1987.

[28] A. Miklós and P. Hess, "Modulated and pulsed photoacoustics in trace gas analysis," *Anal. Chem.*, vol. 72, pp. 30A–37A, 2000.

[29] R. G. Polcawich and P. M. Pellegrino, "Microelectromechanical resonant photoacoustic Cell," U.S. Patent 7 304 732, Dec. 4, 2003.

[30] E. Brunol, F. Berger, M. Fromm, and R. Planade, "Detection of dimethyl methylphosphonate (DMMP) by tin dioxide-based gas sensor: Response curve and understanding of the reactional mechanism," *Sens. Actuators, B*, vol. 120, pp. 35–41, 2006.

[31] T. A. Heumier and J. L. Carlsten, ILX Lightwave Corporation, "App note 8: Mode hopping in semiconductor lasers," Bozeman, MT, 2003.

[32] "Final recommendations for protecting human health from potential adverse effects of exposure to agents GA (Tabun), GB (Sarin) and VX," *Fed. Regist.*, vol. 68, pp. 58348–58350, 2003.

Ellen L. Holthoff received the B.S. degree in chemistry from Lebanon Valley College, Annville, PA, in 2002, and the Ph.D. degree in chemistry from the University at Buffalo, State University of New York, in 2007.

She is currently an Oak Ridge Associated Universities Postdoctoral Fellow at the U.S. Army Research Laboratory, Adelphi, MD. Her research interests include molecularly imprinted polymers and optical sensors.

David A. Heaps received the B.S. degree in chemistry from Brigham Young University, Provo, UT, in 1996, and the Ph.D. degree in chemistry from the University of Idaho, Moscow, in 2005.

Currently, he is a Senior Scientist at AstraZeneca Pharmaceuticals LP, Wilmington, DE. From 2005 to 2007, he held an Oak Ridge Associated Universities Postdoctoral Fellowship at the U.S. Army Research Laboratory (ARL). Experimental work included the design of a MEMS-scale photoacoustic sensor using an interband quantum cascade laser. His research interests include applications of vibrational spectroscopy.

Paul M. Pellegrino received the B.S. degree in physics from Seattle University, Seattle, WA, in 1989, and the M.S. and Ph.D. degrees in physics from New Mexico State University, Las Cruces, in 1993 and 1996, respectively.

He is currently the Team Leader of the Optical Devices and Sensors Team in the Sensors and Electron Devices Directorate, the U.S. Army Research Laboratory (ARL), Adelphi, MD. He was with the ARL, as a Physicist, for approximately nine years. From 1996 to 2000, he held both a National Research Council and an American Society for Engineering Education Postdoctoral Fellowship at ARL. In addition to his team leader duties, he has also involved in the development of a microelectromechanical systems scale photoacoustic sensor platform, originally funded under an ARL Director's Research Initiative. He has more than 18 years experience in the areas of optics, physics, and computational physics, with a strong emphasis in the last 13 years on the application of novel spectroscopy and optical transduction for chemical and biological sensing. Other research interests include a novel terbium photoluminescence technique for detection of bacterial endospores.

Dr. Pellegrino is a member in good standing of both the Optical Society of America and the Society for Applied Spectroscopy.